JOURNAL OF GEOPHYSICAL RESEARCH, VOL. 112, D10108, doi:10.1029/2006JD008191, 2007

Coupling of water vapor convergence, clouds, precipitation, and land-surface processes

Alan K. Betts[1]

Received 27 October 2006; revised 7 January 2007; accepted 1 February 2007; published 19 May 2007.

[1] On daily timescales, the climate over land is a complex balance of many coupled processes. ERA40 reanalysis data for subbasins of the Mississippi in summer are used to explore the links between these processes in a fully coupled model system, and observed surface precipitation and surface short-wave fluxes derived by the International Satellite Cloud Climatology Project are used for evaluation. This paper proposes that the effective cloud albedo viewed from the surface is a useful link which connects the cloud fields to both surface and large-scale processes. The reanalysis has a low bias in cloud albedo in all seasons except summer. In the coupled system in the warm season, on daily timescales, the lifting condensation level falls as soil moisture and precipitation increase. The ratio of the cloud short-wave radiative forcing at the surface to the diabatic precipitation heating of the atmosphere is less in the reanalysis than in the observations. The surface energy budget is split into the surface net radiation and the evaporative fraction. The surface cloud radiative forcing largely determines the surface net radiation, while evaporative fraction, with fixed vegetation, is largely determined by temperature and near-surface soil moisture.

Citation: Betts, A. K. (2007), Coupling of water vapor convergence, clouds, precipitation, and land-surface processes, *J. Geophys. Res.*, *112*, D10108, doi:10.1029/2006JD008191.

1. Introduction

[2] On timescales of a day and space scales of order 800 km, the climate over land is a complex balance of many highly coupled processes. In the atmosphere, water vapor convergence is linked to precipitation and clouds, which in turn modify the radiation fields. Over land the surface energy budget is strongly influenced by the cloud field, and the availability of water for evaporation. Reanalysis data for subbasins of the Mississippi will be used to explore the links between these processes on river basin scales, using for evaluation observed surface precipitation and surface short-wave fluxes derived by the International Satellite Cloud Climatology Project (ISCCP). Clouds play a major role in the climate system through their top-of-the-atmosphere (TOA) impact on the radiative fluxes, where they increase the planetary albedo and typically reduce the outgoing long-wave flux. For more than a decade, cloud radiative forcing in models has been regarded as a major source of uncertainty in modeling climate [*Cess et al.*, 1990]. Yet the TOA radiative effects of clouds are easy to observe from space, and the surface radiative fluxes are routinely derived from them [*Pinker et al.*, 2003]. So given these extensive observational data, which clearly identify model biases in the surface radiation budget [e.g., *Betts et al.*, 2006b], why have corresponding improvements in models not been rapid? This paper proposes that the effective cloud albedo viewed from the surface (which will be defined in section 2.2) is one missing observable link that can be used to connect the cloud fields to both surface and large-scale processes. The cloud fields are a tightly coupled component of the hydrologic cycle and the climate system. Over land, clouds are partly linked locally to the availability of soil water, which impacts evaporation and the lifting condensation level (LCL), and partly linked to large-scale convergence of moisture which generates clouds and precipitation. The system is tightly coupled at the surface because clouds reduce the incoming short-wave and outgoing long-wave radiative fluxes, which generally reduces the energy available to drive evaporation. In addition, some precipitation evaporates as it falls (modifying atmospheric properties including the LCL), some precipitation evaporates rapidly off wet canopies, while some refills the soil water reservoirs (and some runs off).

[3] This paper is one of a series which explores and evaluates the coupling of processes in the European Centre for Medium-Range Weather Forecasts (ECMWF) reanalysis [*Uppala et al.*, 2005] usually known as ERA40. (In fact it covered 45 years from September 1957 to August 2002.) It used the land-surface scheme described by *Van den Hurk et al.* [2000], and a 3-D variational assimilation system. The horizontal resolution of the spectral model is triangular truncation at T_L-159, and there are 60 levels in the vertical, including a well-resolved boundary layer and stratosphere. Documentation of the Integrated Forecast System (IFS), cycle 23r4, and a summary and discussion of the observations available at different times during the 45-year reanalysis can be found at http://www.ecmwf.int/research/era/.

[1] Atmospheric Research, Pittsford, Vermont, USA.

0148-0227/07/2006JD008191$09.00

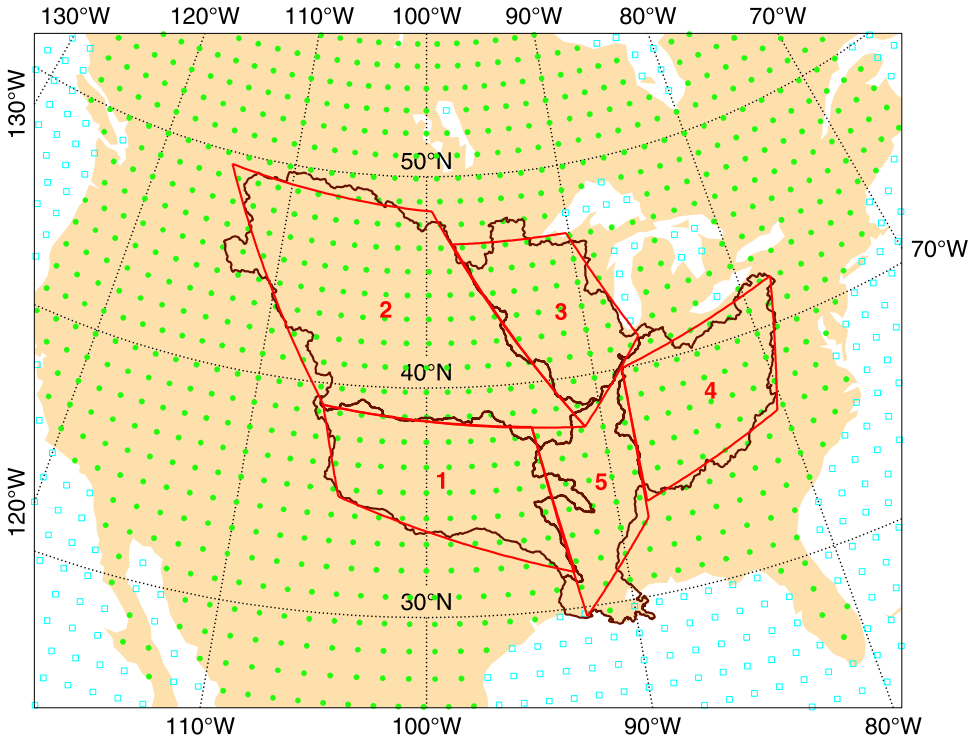

Figure 1. ERA40 river basins for the Mississippi river.

One feature of ERA40 is a special hourly archive [*Källberg et al.*, 2004] at selected points (where there are data from flux towers) and averages over selected river basins of the surface energy and water budgets, as well as the subsurface, near-surface and atmospheric variables. These river basin averages were originally archived to study the hydrometeorology of river basins [e.g., *Betts et al.* 2003a, 2003b, 2005]. However, model data can provide powerful insights into the coupling of physical processes, even though quantitatively there will be dependence on the specific parameterizations of a given model. *Betts* [2004] and *Betts and Viterbo* [2005] used reanalysis data to explore the interrelation of the surface fluxes, the boundary layer, the cloud fields and surface radiation balance on the daily and seasonal timescales in ERA40. *Betts and Viterbo* [2005] also showed the tight relationship between the TOA cloud albedo and the effective cloud albedo viewed from the surface (defined in 2.2 later) for a southwestern basin of the Amazon. *Betts* [2006] looked at the link between the amplitude of the diurnal cycle of temperature and the surface daily mean outgoing long-wave flux from the tropics to high latitudes, again using river basin means from ERA40. *Betts et al.* [2006a] evaluated an hourly grid point time series from ERA40 against many years of data from three forest flux towers in central Saskatchewan, two within the grid box and one adjacent to it. This showed that, while the seasonal biases of temperature and humidity in ERA40 are small, the reanalysis has a high bias in evaporation and a low bias in reflective cloud except in summer. Again, the effective cloud albedo viewed from the surface was used to organize the data. In summer, on days with high observed cloud cover, the model has too little cloud, and a corresponding high sensible heat flux and a warm, dry bias. In contrast, when observed cloud is lower, the model biases are generally reversed. However, while such a grid point comparison with high-quality data can provide great detail, it is always unclear whether the biases of the model can be regarded as representative of larger regions. Moreover, it is difficult to assess model precipitation at a single grid point.

[4] This paper extends this work to the coupling of water vapor convergence, clouds, precipitation and land-surface processes for the midlatitude basins of the Mississippi River, using precipitation observations and the ISCCP surface short-wave flux to evaluate ERA40. With these data, we can estimate the bias in ERA40 of the ratio of the precipitation diabatic forcing of the atmosphere to the surface cloud short-wave radiative forcing. This is a key relationship from a climate and energetic perspective, and it will be one focus of this paper. The second focus of this paper will be to partition the surface energy budget in ERA40 into the available energy, where the variability is largely determined by the variability of surface cloud albedo, and the evaporative fraction, where the variability, given the vegetation parameters, is largely determined by temperature and soil water. This suggests how combinations of satellite data and surface variables may give better estimates of the surface energy budget. However, this aspect of the analysis is only exploratory, since we have neither the sensible and latent heat fluxes nor soil water on the river basin scale for evaluation.

2. Data and Definitions

2.1. Mississippi Basin Data From ERA40

[5] Figure 1 shows the subbasins of the Mississippi river, labeled 1 to 5, representing respectively the Red-Arkansas, the Missouri, Upper Mississippi, Ohio-Tennessee, and the lower Mississippi. During the analysis cycle ERA40 gen-

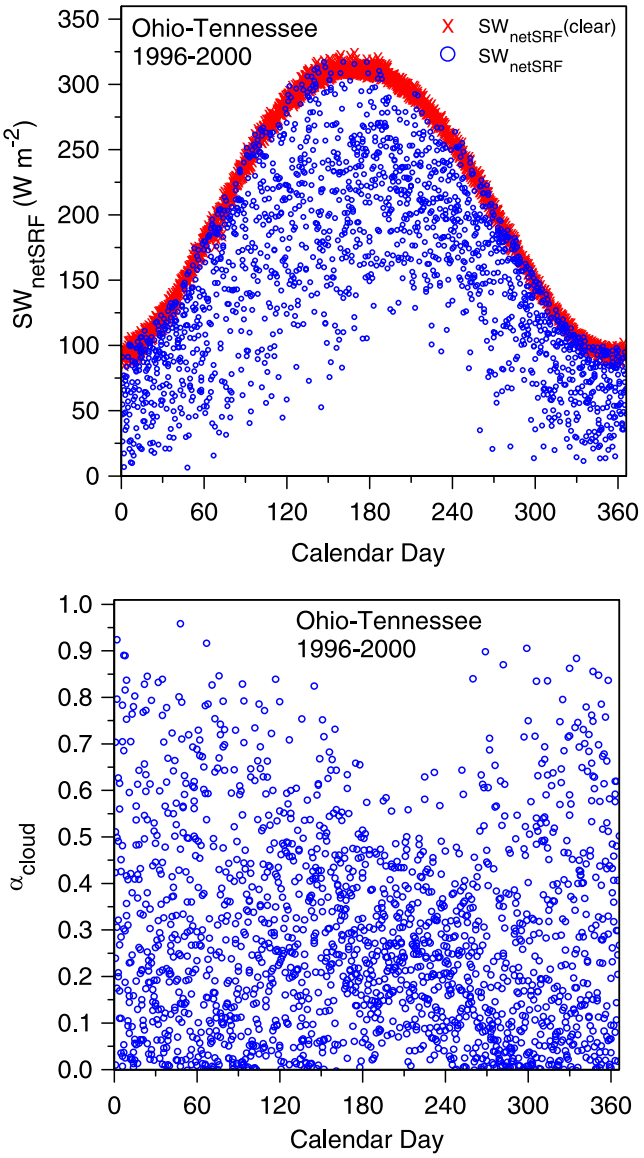

Figure 2. Annual distribution of (top) total and clear-sky SW_{netSRF} and (bottom) effective surface cloud albedo.

erated averages over all grid points (indicated as dots) inside each polygon, which are approximations to the actual river basin boundaries shown. The data period chosen for analysis is from 1983 to 2001, for which there is ISCCP data for comparison. Daily means were derived for each basin by averaging the hourly data from a single 24-hour short-term forecasts from the 0000 UTC analysis. The annual cycle of precipitation and cloud for the basins labeled 1 to 4 will be shown. The analysis will then concentrate on the warm season for only two basins, the Missouri river basin 2 (area of 1.3×10^6 km^2) and Ohio-Tennessee basin 4 (area of 0.46×10^6 km^2), taking these two as representative of the drier central and the wetter eastern United States respectively. There are differences in the model vegetation between the Ohio-Tennessee basin, which is over 85% forested, and the Missouri basin for which forest cover is less than 15%. There is no seasonal cycle in the vegetation parameters in ERA40.

[6] The analysis here is in terms of daily means, as in the work by *Betts et al.* [2006a]. The advection distance in 24 hours at 10 m s^{-1} is 864 km. This corresponds to roughly 10° of longitude at 40°N, which roughly lies between the spatial scales of the Ohio-Tennessee and Missouri river basins (see Figure 1). ERA-40 does have errors in the diurnal cycle of precipitation, typically precipitation occurs too early in the diurnal cycle [see *Betts and Jakob*, 2002], but these will not be explored here.

2.2. Definition of Effective Surface Cloud Albedo

[7] The ERA40 archive [*Kållberg et al.*, 2004] contains net "clear-sky" fluxes (surface, SRF, and top-of-the-atmosphere, TOA) computed without the model cloud field, as well as the radiation fluxes computed with the model (prognostic) cloud field. The cloud forcing (CF) terms can be computed from these net SW and LW fluxes by difference. At the surface, the short-wave cloud forcing is defined as the difference of the surface net short-wave all-sky and clear-sky fluxes (both defined as positive downward)

$$\mathrm{SWCF_{SRF}} = \mathrm{SW_{netSRF}} - \mathrm{SW_{netSRF}(clear)} \tag{1}$$

so that the $SWCF_{SRF}$ is negative. The surface effective cloud albedo is defined as

$$\alpha_{\mathrm{cloud}} = -\mathrm{SWCF_{SRF}}/\mathrm{SW_{netSRF}(clear)} \tag{2}$$

so that the SW surface budget can be written in the symmetric form

$$\mathrm{SW_{netSRF}} = (1-\alpha_s)(1-\alpha_{\mathrm{cloud}})\mathrm{SW_{dnSRF}(clear)} \tag{3}$$

where SW_{dnSRF} is the downward SW flux at the surface. The albedo of the underlying surface, α_s, (assumed the same for both the clear-sky and all-sky fluxes) satisfies both

$$\begin{aligned}\alpha_s &= (\mathrm{SW_{dnSRF}} - \mathrm{SW_{netSRF}})/\mathrm{SW_{dnSRF}} \\ &= (\mathrm{SW_{dnSRF}(clear)} - \mathrm{SW_{netSRF}(clear)})/\mathrm{SW_{dnSRF}(clear)}\end{aligned} \tag{4}$$

The total cloud forcing at the surface is

$$\mathrm{CF_{SRF}} = \mathrm{SWCF_{SRF}} + \mathrm{LWCF_{SRF}} \tag{5}$$

where the LW cloud forcing is defined in a similar manner as

$$\mathrm{LWCF_{SRF}} = \mathrm{LW_{netSRF}} - \mathrm{LW_{netSRF}(clear)} \tag{6}$$

The LW_{net} terms are both negative, while their difference $LWCF_{SRF}$ is positive. The transformation represented by (1) and (2) is illustrated in Figure 2 for five years of daily mean data for the Ohio-Tennessee river basin. Figure 2 (top) shows SW_{net}, as a distribution of scattered points below SW_{netSRF}(clear), which form an upper envelope. The difference, $SW_{netSRF} - SW_{netSRF}$(clear) is the SW cloud forcing given by (1) and it is always negative. Figure 2 (bottom) shows the effective cloud albedo from (2), which always satisfies $0 < \alpha_{cloud} < 1$. This transformation removes the large seasonal variation of clear-sky fluxes associated with changing solar zenith angle. The range of effective

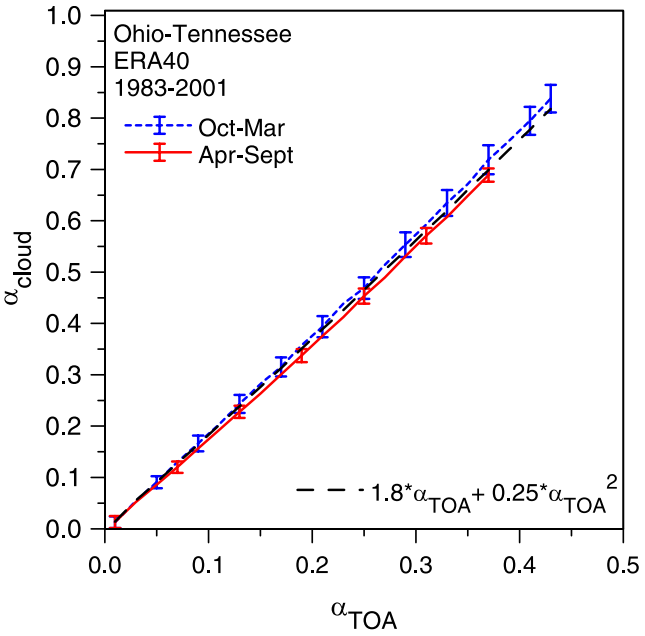

Figure 3. Relation of effective surface cloud albedo to TOA cloud albedo.

cloud albedo is greater in winter than in summer for this basin. α_{cloud} is an "effective" surface cloud albedo, because it represents the fraction of the clear-sky flux that does not reach the surface because of the cloud field. Thus it includes both the reflection and the smaller absorption by the cloud field. For brevity however it will be called surface cloud albedo. *Eltahir and Humphries* [1998] use a similar concept to quantify the SW cloud forcing over the Amazon by normalizing the reduction in the incoming SW flux by the observed range between clear and totally cloudy skies.

2.3. Relation of Surface and TOA Cloud Albedos

[8] The TOA cloud albedo is related to the TOA cloud forcing by

$$\alpha_{TOA} = -\mathrm{SWCF}_{TOA}/\mathrm{SW}_{dnTOA}(\mathrm{clear}) \quad (7)$$

where the TOA SW cloud forcing is defined as

$$\mathrm{SWCF}_{TOA} = \mathrm{SW}_{netTOA} - \mathrm{SW}_{netTOA}(\mathrm{clear}) \quad (8)$$

Figure 3 shows the relation of the TOA cloud albedo from (7) to the effective surface cloud albedo, defined by (2). The daily mean data have been binned by α_{TOA} and by warm and cold seasons. For visual reference, a quadratic relationship

$$\alpha_{cloud} = 1.8\ \alpha_{TOA} + 0.25\ \alpha_{TOA}{}^2 \quad (9)$$

is plotted as a heavy dashed line. In ERA40, the relationship between TOA and effective surface cloud albedos varies only a little by season and between river basins (not shown). Note also that the standard deviations of the daily data, averaged over the Ohio-Tennessee basin, while small, are a little larger in the cold season, when the clear-sky solar fluxes are smaller. These cloud albedos are useful quantitative measures of the cloud field. In this section, they are derived from the model cloud fields, but they are also readily derived from satellite data (see next section).

2.4. Evaluation Data

[9] Two sets of observationally based data are used for model evaluation. "Observed" surface cloud albedos were derived from the daily means of the ISCCP SW_{dnSRF} fluxes [*Zhang et al.*, 1995; *Rossow and Zhang*, 1995] averaged over the Mississippi basins [see *Betts et al.*, 2003a] using the ERA40 SW_{dnSRF}(clear). The radiative model, atmospheric composition and aerosol structure used for the ISCCP retrievals are outlined in detail by *Zhang et al.* [1995]. The atmospheric temperature and moisture profiles come from the TIROS operational vertical sounder daily analysis [*Smith et al.*, 1979]. For ERA40, atmospheric temperature and moisture structure comes from the 3-D variational assimilation of a wide range of data, including satellite microwave and infrared radiances as well as in situ data. Details of the SW radiation model and aerosol climatology used are given by *Morcrette* [2002]. Since the models differ in their SW radiation schemes, and treatment of aerosols, their computation of the clear-sky fluxes also differ. This requires more detailed analysis, which is left for future work. Since we use only the ERA40 clear-sky fluxes as a reference, the estimate of effective cloud albedo from the ISCCP data implicitly contains a small bias related to the differences in the computation of the clear-sky fluxes. Nonetheless, in comparing effective cloud albedos, we are still comparing the SW_{dnSRF} fluxes between ERA40 and ISCCP. The surface LW fluxes computed by ISCCP will not be used, as these are sensitive to errors in surface temperature and lower tropospheric temperature profiles [*Betts et al.*, 2003a].

[10] For precipitation, the 2 × 2.5° gridded hourly [*Higgins et al.*, 1996] and 0.25° gridded daily [*Higgins et al.*, 2000] products from the National Climatic Data Center (NCDC) were averaged over the Mississippi subbasins and then compared on the monthly timescale. The daily product has a higher native resolution, as it uses many more rain gages than the hourly product, and has greater precipitation in all seasons, and it is thought to be the better product. However, the "24h-day" starts and ends at 1200 UTC (when most of the daily gages are read), whereas in all our other analyses the day runs from 0000 to 2400 UTC. So a daily mean was derived from the hourly precipitation data and then the precipitation was scaled upward with a mean monthly weighting function to match the monthly mean from the gridded daily product. One complication is that the ratio of precipitation from the daily and hourly products shows a clear increase (probably due to changes in the hourly network instrumentation) between 1996 and 1998 (largest for the Missouri river basin), so we identified an approximate transition date for each basin and used separate mean monthly weighting functions before and after.

3. ERA40 Seasonal Bias of Cloud and Precipitation

3.1. ERA40 Cloud Albedo Bias

[11] The upper curves in Figure 4 show the mean seasonal cycle of the effective cloud albedo for four Mississippi subbasins, derived from the ISCCP data SW_{dnSRF}, using (1)

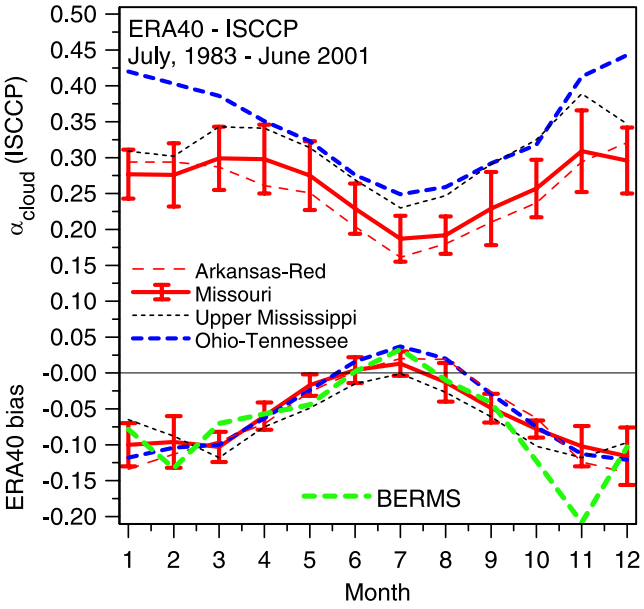

Figure 4. Mean seasonal cycle of ISCCP surface cloud albedo and ERA40 bias. The bias against BERMS flux tower sites is also shown.

and (2) and the ERA40 SW_{netSRF}(clear). The lower curves are the ERA40 α_{cloud} bias, defined as α_{cloud}(ERA40) – α_{cloud}(ISCCP). ERA40 has a systematic bias structure with too little reflective cloud except in summer. This albedo bias in the reanalysis is as large as −10% in winter. A representative set of standard deviations of the monthly means are shown for one basin: note that typically the variability of the model bias is less than the interannual variability of the observed cloud albedo. This seasonal bias pattern in cloud albedo is very similar to that found in a comparison study [*Betts et al.*, 2006a] with the three Boreal Ecosystem Monitoring Study (BERMS) flux tower sites in central Saskatchewan, which is shown as a heavy dashed line.

[12] Figure 5 shows the distribution of days with a given cloud albedo in winter (Figure 5a) and in summer (Figure 5b) for the ISCCP data, and the bias, ERA40-ISCCP. In winter ERA40 has many more days with very little cloud and many fewer days in every cloud albedo class >0.2. This pattern suggests that ERA40 underestimates cloud cover (see Figure 6). In summer, the ERA40 bias pattern is smaller, and the ISCCP distributions are more peaked in the range 0.1–0.2, with generally fewer clear days than ERA40.

3.2. Daily Scatterplots of Albedo Bias

[13] Figure 6 compares daily ERA40 cloud albedo with ISCCP for the Ohio-Tennessee basin for the four seasons (winter is December, January, February etc). The scatter between observations and reanalysis is relatively small on the daily timescale, only ±0.1, but the systematic seasonal biases are clearly visible. In winter, ERA40 has a low cloud bias on almost all days, except when it is very cloudy. The bias is smaller in spring and fall, while in summer there is a small high bias, as shown in Figure 4.

3.3. ERA40 Precipitation Bias

[14] Figure 7 shows the annual cycle of the observed NCDC precipitation and the bias, ERA40 – NCDC. The standard deviations of the monthly means shown for the Missouri river basin are typical: note that the interannual variability of precipitation is larger than the variability of the bias. The reanalysis precipitation bias for most basins is weakly positive in winter. In summer, the Ohio-Tennessee basin (and the lower Mississippi, not shown) has a high precipitation bias quite different from the other three basins. Comparing Figures 4, 6 and 7 it is clear that in winter ERA40 has too low a cloud albedo, but generally a positive precipitation bias. This clearly suggests that the large-scale precipitation process in the model, which is dominant in winter, is too efficient in its removal of cloud water and ice.

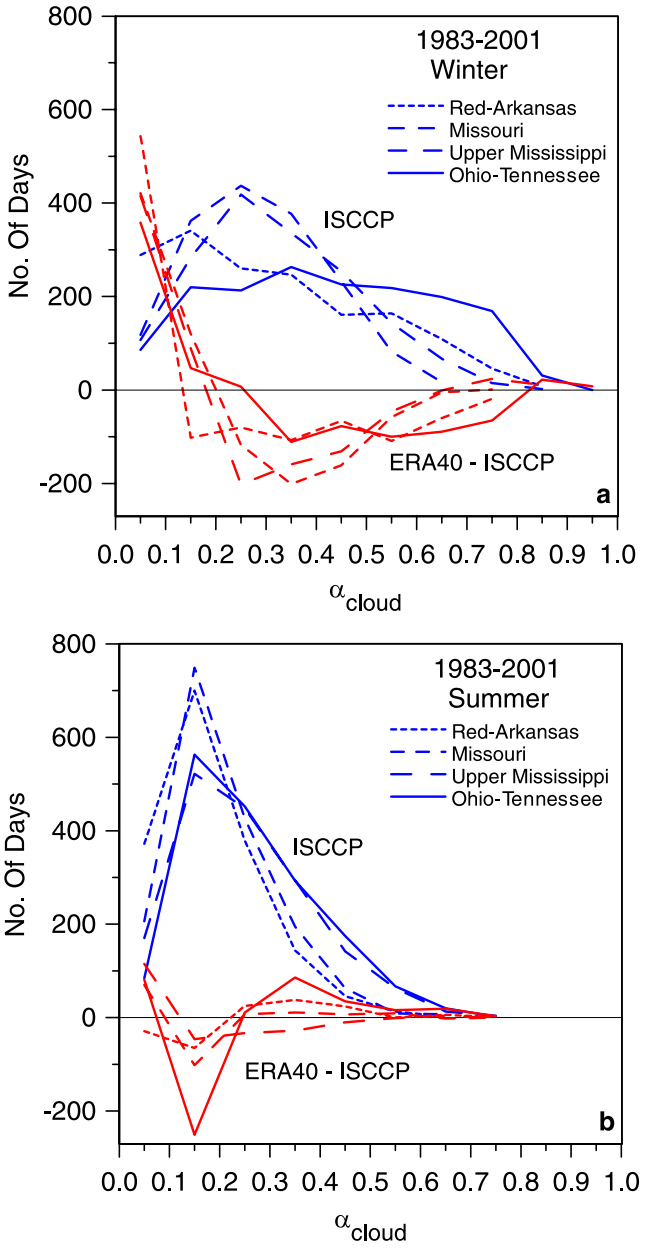

Figure 5. Number of days with a given cloud albedo (a) in winter and (b) in summer for the ISCCP data and the ERA40 bias.

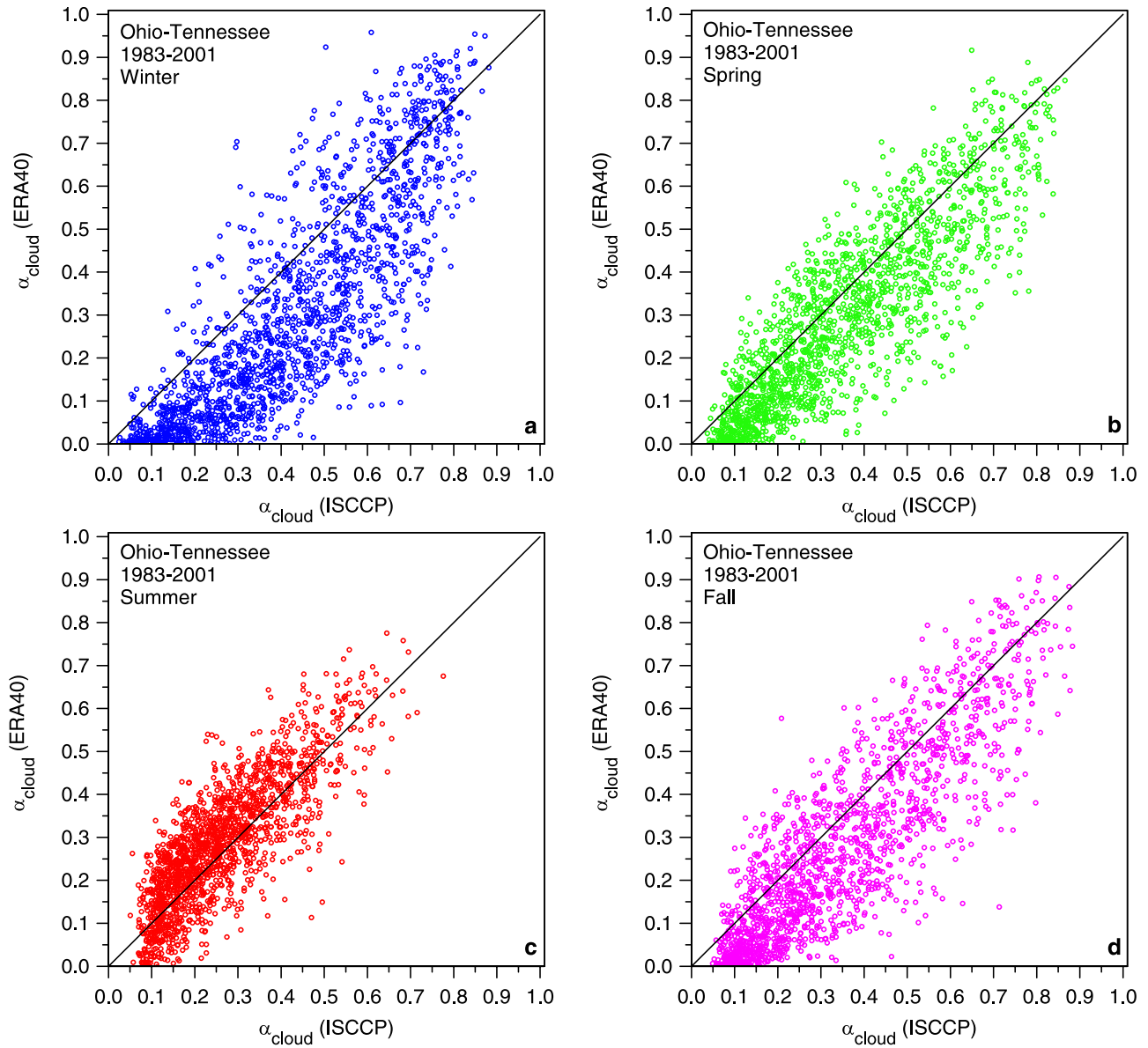

Figure 6. Scatterplot of daily mean cloud albedo for ERA40 against ISCCP for the Ohio-Tennessee river basin for winter, spring, summer and fall.

One caveat is that during the first 24 hours of the ERA40 short-term forecasts, while cloud albedo changes little, the spinup of precipitation is considerable [*Betts et al.*, 2003a, 2003b], so the ERA40 24h forecast precipitation may have a low bias, of order 10%. However, precipitation analyses also tend to have a low bias of this order, resulting from gage undercatch.

4. Warm Season Links Between Moisture Convergence, Cloud, and Precipitation

4.1. Analysis Strategy

[15] Figure 4 shows that ERA40 has a seasonal bias in surface effective cloud albedo, which is small in the warm season months, May–August, when land-surface processes play an important role in the land-boundary layer-atmosphere coupling [*Betts et al.*, 1996]. The model data set was analyzed, looking for relationships between surface precipitation, cloud radiative forcing, CF_{SRF}, and other variables using α_{cloud} as a measure of the cloud field. The daily basin averages of effective cloud albedo, derived from the ISCCP data, and precipitation from the NCDC data were used for evaluation. The land-boundary layer-atmosphere system is highly coupled one, and while the figures that will be shown are suggestive of important couplings within the system on the daily timescale, they do not show a "direction of causality." Nonetheless, they will show that the surface cloud SW radiative forcing in ERA40 has a low bias in summer when compared with the diabatic precipitation forcing of the atmosphere.

[16] Three parameters were taken from the reanalysis to additionally stratify the data. Large-scale forcing was represented quantitatively by the daily mean vertically integrated moisture convergence, VIMC, for each basin, generated from the four analysis times. Moisture convergence is clearly associated with clouds and precipitation.

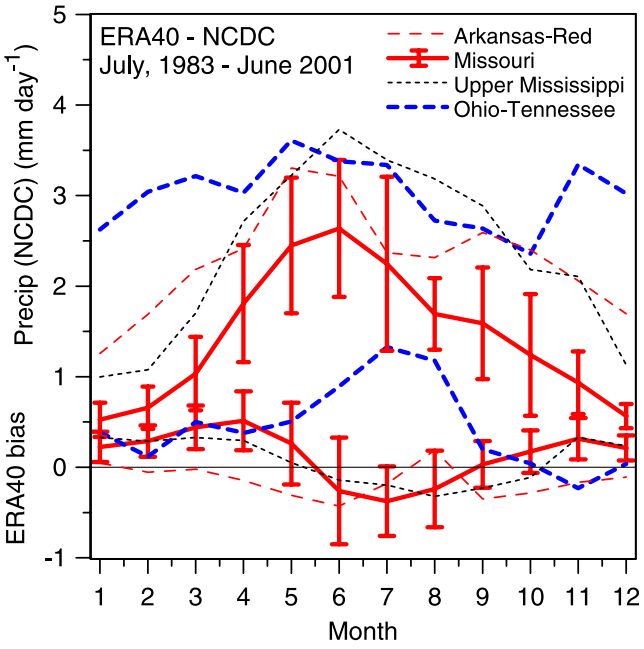

Figure 7. Mean seasonal cycle of NCDC precipitation and ERA40 bias.

[17] As an indicator of the boundary layer equilibrium on daily timescales [see *Betts*, 2004], and an estimate of the mean height of cloud base, the height of the lifting condensation level (LCL) in pressure coordinates, P_{LCL}, was computed from the lowest model level data (about 10 m above the surface). P_{LCL} is closely related to near-surface relative humidity, RH, at this model level [see *Betts*, 1997; *Betts et al.*, 2006a].

[18] A soil moisture index was computed for the first 0–7 cm soil layer as

$$\text{SMI-L1} = (\text{SM} - 0.171)/(0.323 - 0.171) \qquad (10)$$

where SM is the model soil water fraction, the model soil permanent wilting point is 0.171 and the model field capacity is 0.323. SMI-L1 is not only a useful index on the daily timescale for the availability of water for evaporation (although transpiration depends also on soil water in deeper layers), but it also responds to precipitation on this timescale. Thus the soil moisture-atmosphere coupling is a two-way interaction. In ERA40 there is in addition a surface analysis of both 2-m temperature and RH, and soil moisture. ERA40 uses an optimal interpolation of soil water [*Douville et al.*, 2000], which adds soil water increments based on analysis increments in 2-m temperature and RH. The intent is to minimize errors in the diurnal cycle of these 2-m variables. These soil water increments are small on the daily timescale (<1 mm), but they constrain long-term drifts in soil water in the analysis.

4.2. Interrelationship of Soil Moisture, Lifting Condensation Level, RH, and Precipitation

[19] Earlier papers [*Betts*, 2004; *Betts and Viterbo*, 2005] have shown the strong link between soil moisture index and P_{LCL} in ERA40. *Dirmeyer et al.* [2006] has shown evidence that this relationship is generally supported by observations, although a very wide range of behavior was seen in the models they studied from the Global Land-Atmosphere Coupling Experiment. Figure 8 shows this relationship is dependent in ERA40 on daily precipitation rate (PR). Near-surface RH is shown (with slight approximation) on the right-hand scale. LCL decreases and RH increases as SMI and precipitation increase, and the relationships are similar for both basins. A representative set of standard deviations of the daily data in shown for one PR. The coupling shown in Figure 8 has several aspects. Soil moisture, especially in the upper soil layer responds directly to precipitation. Evaporation from the surface increases with increasing soil moisture (as well as when there is water in the skin reservoir) and this increases RH and lowers the LCL. In addition the evaporation of falling precipitation lowers the LCL by bringing the subcloud layer closer to saturation, and this effect increases with increasing daily precipitation rate. In addition to these physical relationships, the near-surface analysis of RH is constrained by observations in two ways: indirectly through the soil moisture analysis, discussed in 4.1, which uses analysis increments of 2-m temperature and RH, and during the daytime the surface RH observations are

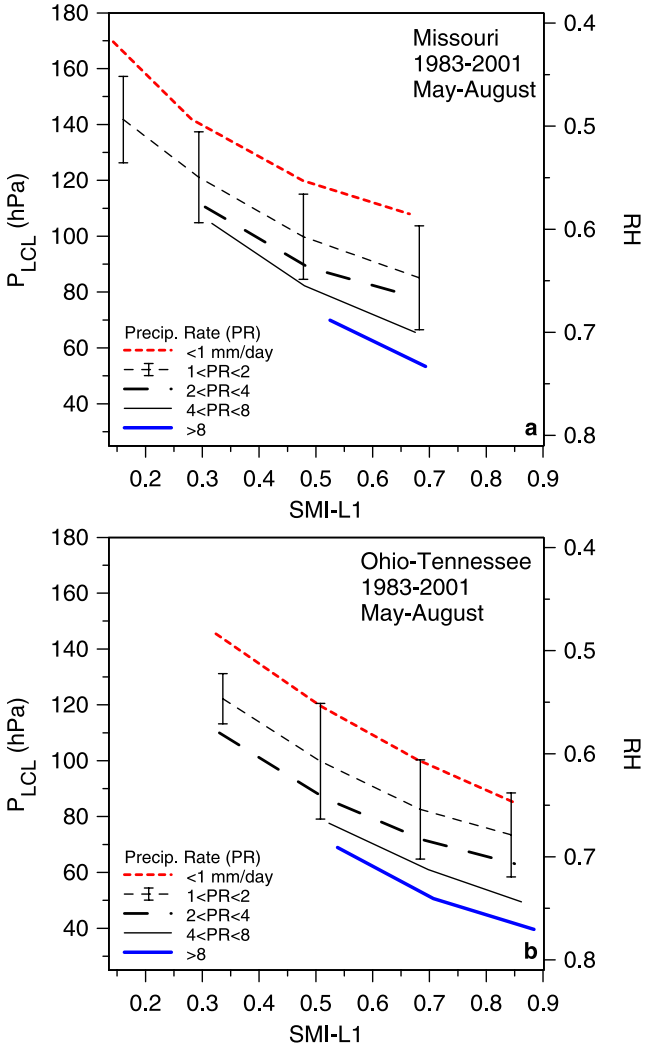

Figure 8. Link between soil moisture index, P_{LCL}, and RH, stratified by daily precipitation rate.

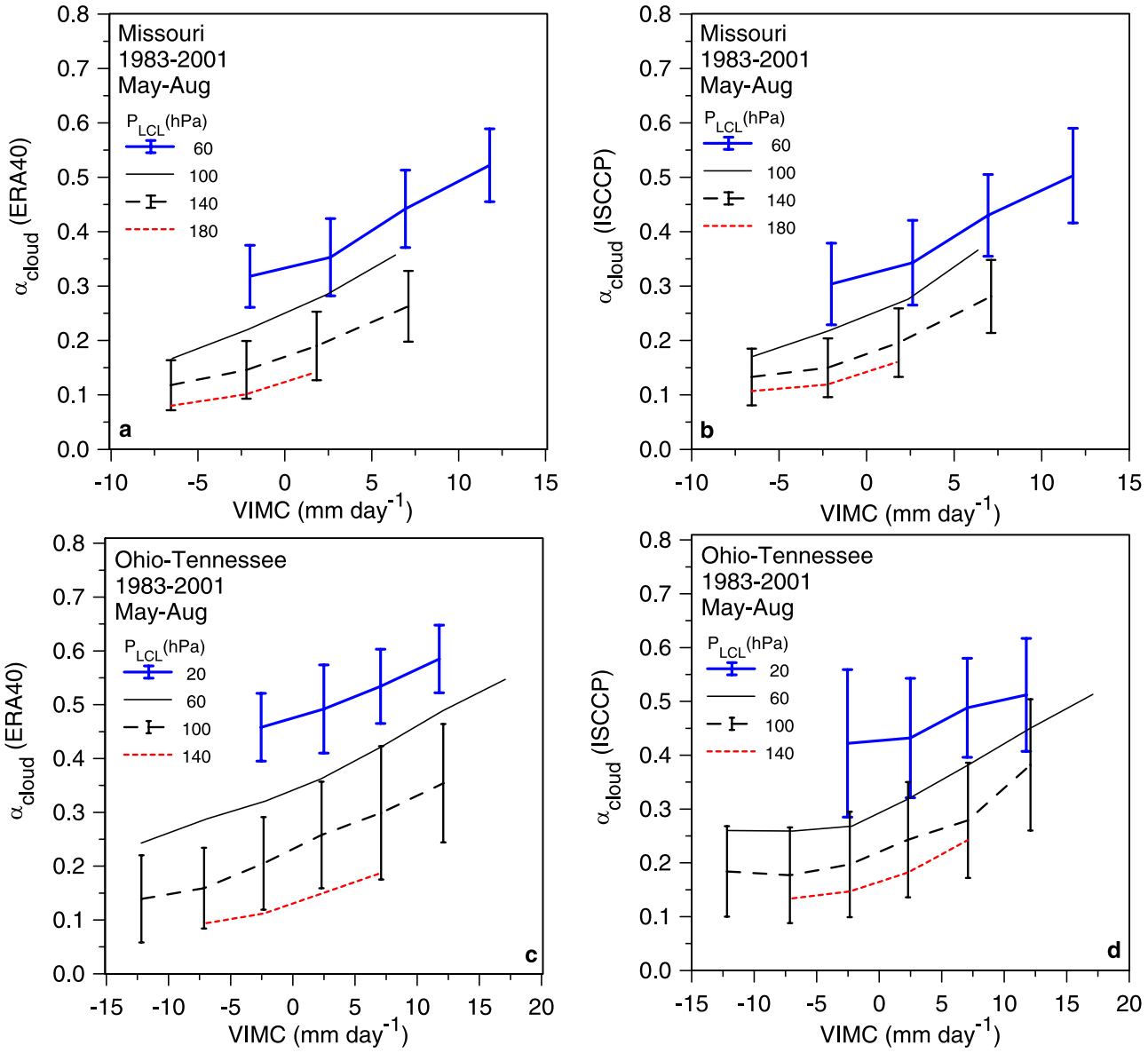

Figure 9. ERA40 and ISCCP cloud albedos as a function of moisture convergence and P_{LCL}.

used directly in the atmospheric 3-D variational assimilation. Consequently, the analysis of RH is constrained in regions of data by the surface humidity observations. As a result the partition of the data by P_{LCL}, which is related to lowest model level RH, proves to be useful.

4.3. Relationship of Cloud Albedo and Precipitation to Moisture Convergence and Cloud Base

[20] Figure 9 shows the relation of the surface cloud albedo in ERA40 (Figures 9a and 9c) and the ISCCP data (Figures 9b and 9d) for the Missouri and Ohio-Tennessee basins, stratified by the two model quantities: vertically integrated moisture convergence, VIMC (bins of 5 mm day^{-1}), and P_{LCL} (40 hPa bins), an estimate of the daily mean cloud base. Not surprisingly, α_{cloud} increases with moisture convergence and a lower cloud base. Observed and model distributions are rather similar, especially for the western Missouri basin. In general, the spread in the ISCCP cloud albedo is lower than in ERA40. The representative standard deviations shown are smaller for the Missouri basin, which has about three times the area of the Ohio-Tennessee basin. Since α_{cloud} is derived from the incoming surface short-wave radiation from completely independent sources, the general agreement in Figure 9 is encouraging.

[21] Figure 10 shows that ERA40 and NCDC precipitation for the same river basins also increases with moisture convergence and decreasing cloud base in a similar manner. When cloud base is high, precipitation is small. As cloud base lowers, the slope of precipitation with moisture convergence becomes steeper. The spread of precipitation with P_{LCL} is a little less in the NCDC data than in ERA40, and the greater precipitation for the Ohio-Tennessee basin in ERA40, seen in Figure 7, is apparent.

4.4. Stratification of Precipitation by Cloud Albedo and P_{LCL}

[22] Figures 9 and 10 show similar dependencies for precipitation and cloud albedo. Figure 11 maps the rela-

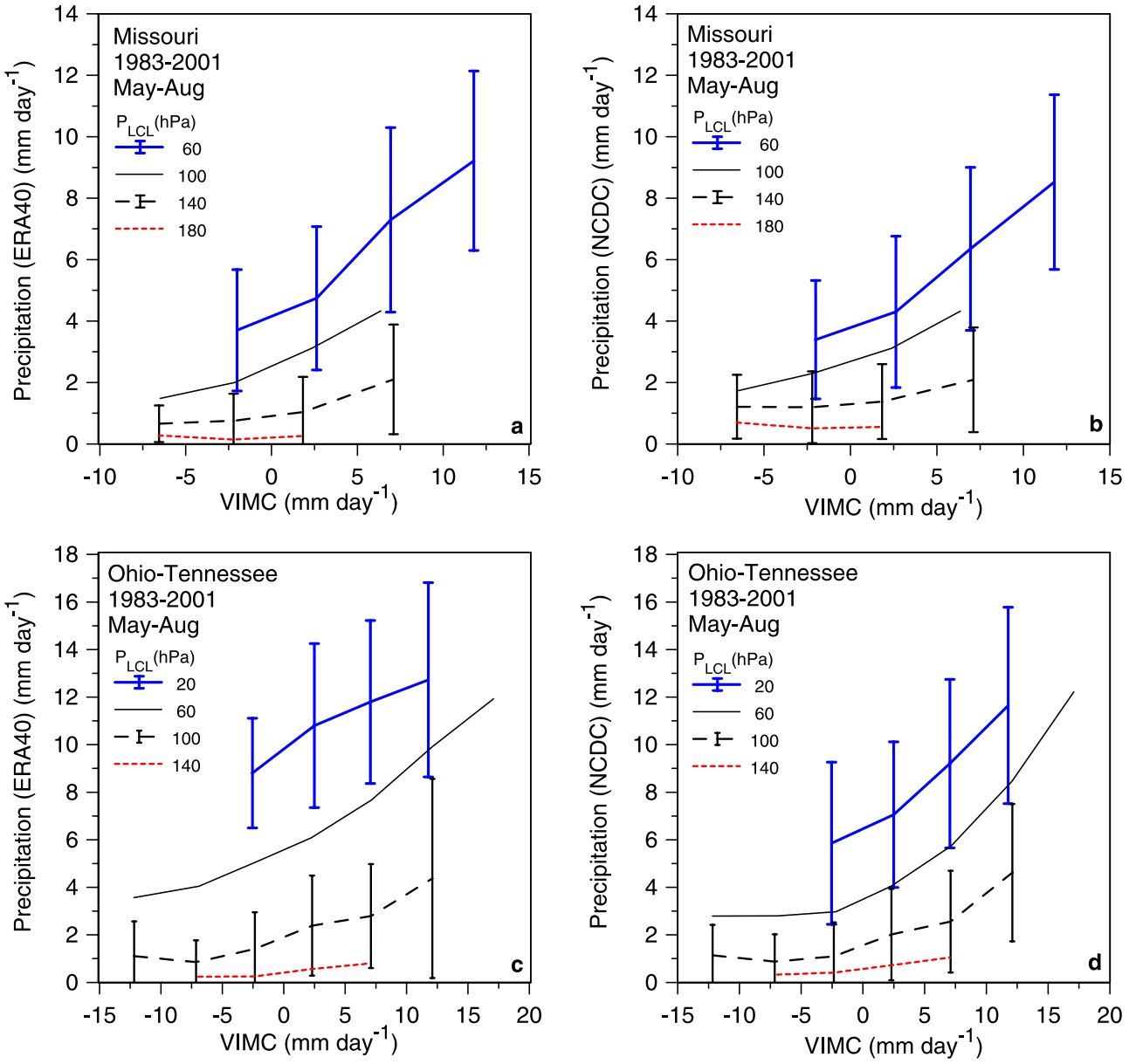

Figure 10. ERA40 and NCDC precipitation as a function of moisture convergence and P_{LCL}.

tion of precipitation to cloud albedo stratified by reanalysis P_{LCL} for both model (Figures 11a and 11c) and observations (Figures 11b and 11d). Some representative standard deviations are shown. More cloud and greater precipitation is linked to both greater α_{cloud} and lower mean LCL. The coupling of precipitation with LCL again goes both ways. A lower LCL is associated with a higher saturation mixing ratio at cloud base (and therefore the likelihood of more precipitation), and the evaporation of falling precipitation lowers the LCL. Nonetheless, this suggests that knowledge of the near-surface LCL provides additional information in the determination of say precipitation from satellite radiances. For the Missouri basin, the variation of observed precipitation with observed cloud albedo is noticeably less steep than the corresponding relation in ERA40. This increases the ratio of the surface cloud SW radiative forcing to the diabatic precipitation forcing of the atmosphere.

4.5. Relation of Cloud Radiative Forcing to Cloud Albedo and Precipitation Heating

[23] The relationship between the surface cloud radiative forcing and the diabatic forcing of the atmosphere by precipitation heating is of fundamental importance to the land-surface-atmosphere coupling. It is also important over the oceans in climate models, but this link is broken in ERA40, as the sea surface temperature is specified. There are long-wave and short-wave components to the cloud surface radiative forcing. The long-wave cloud forcing depends on atmospheric temperature and moisture structure as well as the cloud field. Figure 12a shows the relationship between daily mean P_{LCL}, the mean clear-sky LW_{netSRF} (clear) and the surface all-sky LW_{netSRF}, stratified by cloud

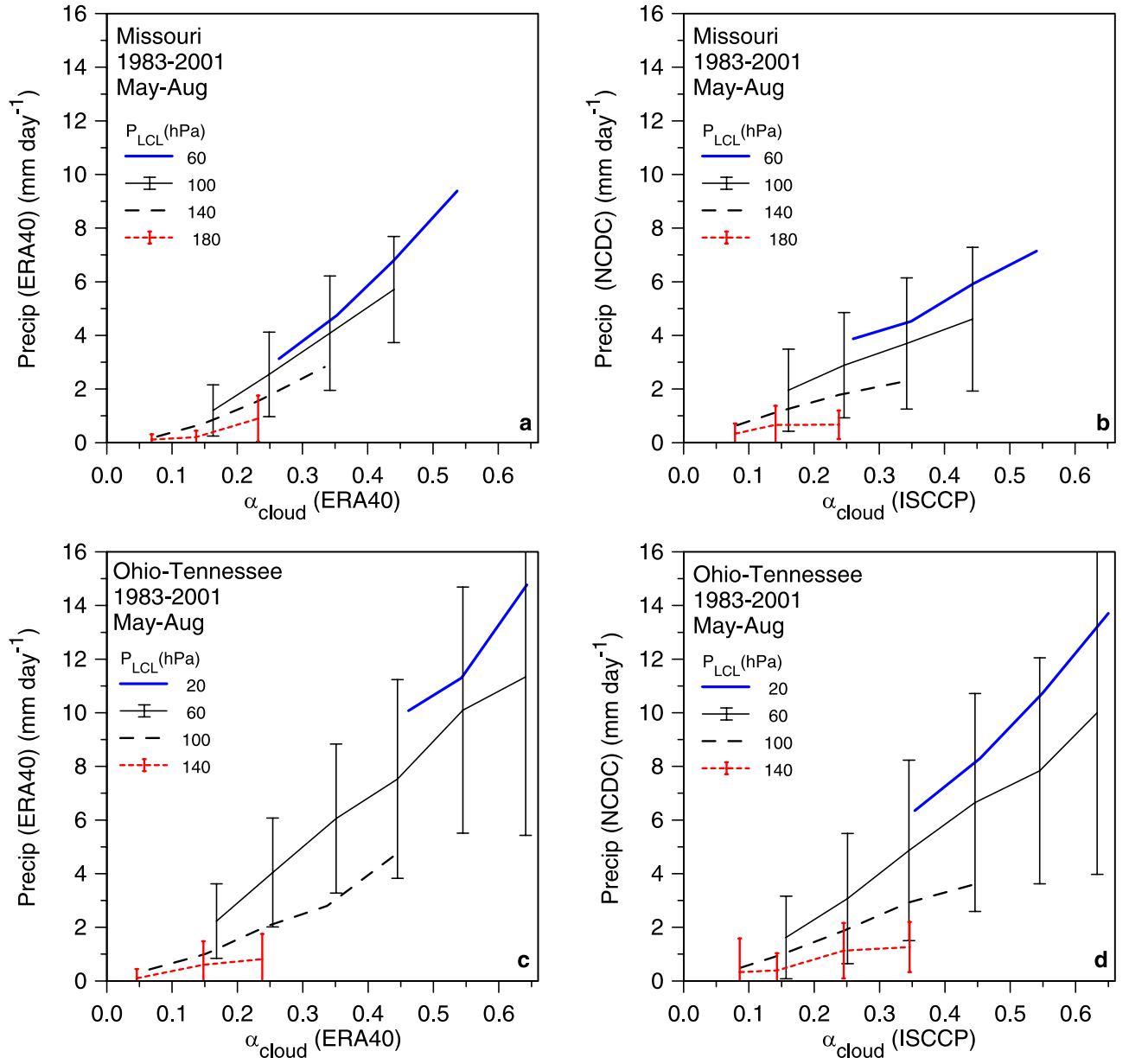

Figure 11. Relation between precipitation and cloud albedo, stratified by P_{LCL} for (left) ERA40 and (right) for observations.

albedo. In ERA40, LW_{netSRF}(clear), the lowest curve, varies with the LCL, which is also related to the low-level RH as seen in Figure 8. A higher mean cloud base gives a larger outgoing LW_{netSRF}(clear). The outgoing all-sky LW_{netSRF} (upper curves) decreases further with increasing α_{cloud}. The $LWCF_{SRF}$, defined by (6) as the difference, varies primarily with α_{cloud}. As a result, the surface total cloud forcing, CF_{SRF} shown in Figure 12b, is almost a linear function of α_{cloud} with no dependence on LCL. The Missouri basin is similar (not shown), except that for the same α_{cloud}, CF_{SRF} is a little smaller in magnitude for the Missouri. There are two reasons for this: the Missouri basin has a higher mean latitude, so that the mean SW fluxes are a little smaller, and the atmosphere over the Missouri is drier, so that the outgoing net LW fluxes are a little larger in magnitude. The comparison by *Betts et al.* [2006a] of surface LW_{net}, stratified by cloud albedo, showed excellent agreement between ERA40 and flux tower observations. The ISCCP surface LW fluxes are not good enough to repeat this evaluation here [*Betts et al.*, 2003a].

[24] However, the short-wave component is a linear function of α_{cloud} through (2), so the relation of the surface SW forcing to precipitation in the reanalysis can be evaluated with the ISCCP data. Figure 13 remaps the stratification of precipitation by α_{cloud} and P_{LCL} in Figure 11 to show the relationship of precipitation diabatic heating (in W m^{-2}) to the surface SW cloud forcing. ERA40 is on the left for the Missouri and Ohio-Tennessee basins, and on the right is the corresponding relation between the NCDC precipitation and the ISCCP cloud SW forcing. Representative standard

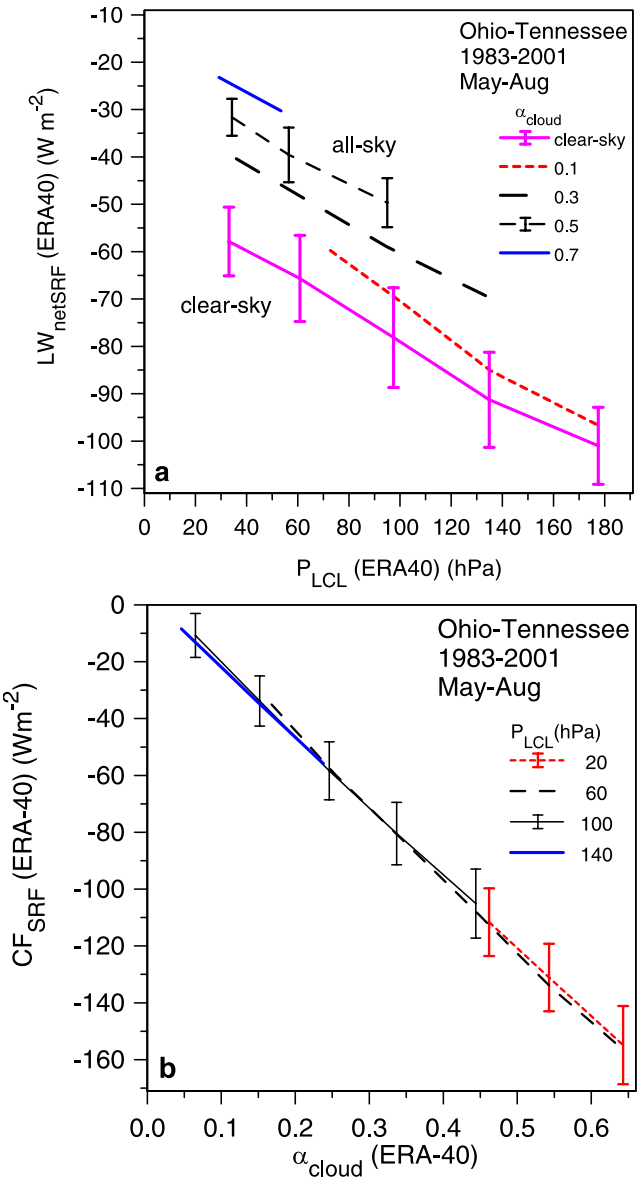

Figure 12. (a) Relation of all-sky and clear-sky LW_{netSRF} to P_{LCL} and α_{cloud}. (b) Surface cloud radiative forcing dependence on α_{cloud} and P_{LCL}.

deviations of the daily data are shown. Note that it is precipitation that has the strong dependence on P_{LCL} (see Figures 8 and 10), not cloud forcing (see Figure 12), but the variability of precipitation is rather large. The relationships are similar for both basins, with a larger range of cloud forcing and precipitation for the Ohio-Tennessee, as seen before. For the Ohio-Tennessee, the reanalysis and the observations are similar. For example, for the Ohio-Tennessee basin for P_{LCL} = 60 hPa, the ratio $(SWCF_{SRF})$/Precip ≈0.51 for reanalysis and ≈0.58 for observations. For the Missouri basin, the difference in this ratio is larger: approximately 0.48 for the reanalysis and ≈0.74 for the observations. This ratio of the diabatic impact of clouds at the surface to that in the atmosphere is an important climate parameter, and it appears that ERA40 has a low bias in summer, when the SW cloud forcing dominates. In winter, ERA40 also has a significant negative bias in cloud albedo, shown in Figure 4, but $SWCF_{SRF}$ is smaller in winter at higher solar zenith angles, and we have not evaluated the corresponding $LWCF_{SRF}$.

5. Links Between Cloud Albedo, Soil Moisture, and Surface Energy Budget in ERA40

[25] The reanalysis data can give some insight into how well the surface energy budget (SEB) might be constrained by satellite observations. The SEB can be divided conceptually into the surface net radiation, R_{netSRF}, and evaporative fraction, EF, defined as

$$EF = \lambda E/(H + \lambda E) \tag{11}$$

where H and λE are the surface sensible and latent heat fluxes.

5.1. Surface Net Radiation

[26] The surface cloud radiative forcing plays an dominant role in the variation of surface net radiation, R_{netSRF}. The partition of net radiation into clear-sky flux and cloud forcing

$$R_{netSRF} = R_{netSRF}(clear) + CF_{SRF} \tag{12}$$

is shown in Figure 14, as a function of α_{cloud} and SMI-L1. The clear-sky fluxes (upper curves) decrease slightly with drier soils and less cloud cover, while cloud forcing is almost a linear decreasing function of α_{cloud} (as already seen in Figure 12b for the P_{LCL} partition). So the variation of R_{netSRF} is dominated by the cloud radiative forcing, which in turn depends on α_{cloud}, which is related to α_{TOA}, as shown in Figure 3.

5.2. Surface Fluxes and Evaporative Fraction

[27] Figure 15 shows the relationship of evaporative fraction EF, to temperature and soil moisture index. As expected, EF increases sharply with SMI, because λE increases and H decreases, and also with temperature. Note that for the Ohio-Tennessee, soil moisture values, EF and the standard deviations are larger than for the Missouri river basin. For reference, Figure 15 also shows the slope with temperature of the classic "equilibrium evaporation" relation [*Priestley and Taylor*, 1972; *McNaughton*, 1976], defined as

$$\text{Equilibrium evaporation} = \beta/(1 + \beta) \tag{13}$$

where $\beta = (\lambda/C_p)\,(\partial q_s/\partial T)_p$ is related to the slope of the Clausius-Clapyron equation at constant pressure, taken here as the mean surface pressure, 900 hPa for the Missouri and 976 hPa for the Ohio-Tennessee. The relations for EF are similar for the two basins, despite the differences in the model vegetation parameters; the Ohio-Tennessee is over 85% forested, while the Missouri forest cover is less than 15%. The rather sharp partition of daily mean EF by near-surface (0–7 cm) soil moisture in ERA40 would suggest that useful information on EF might be determined from temperature and microwave estimates of near-surface soil water. ERA40 however has a simplified land-surface model

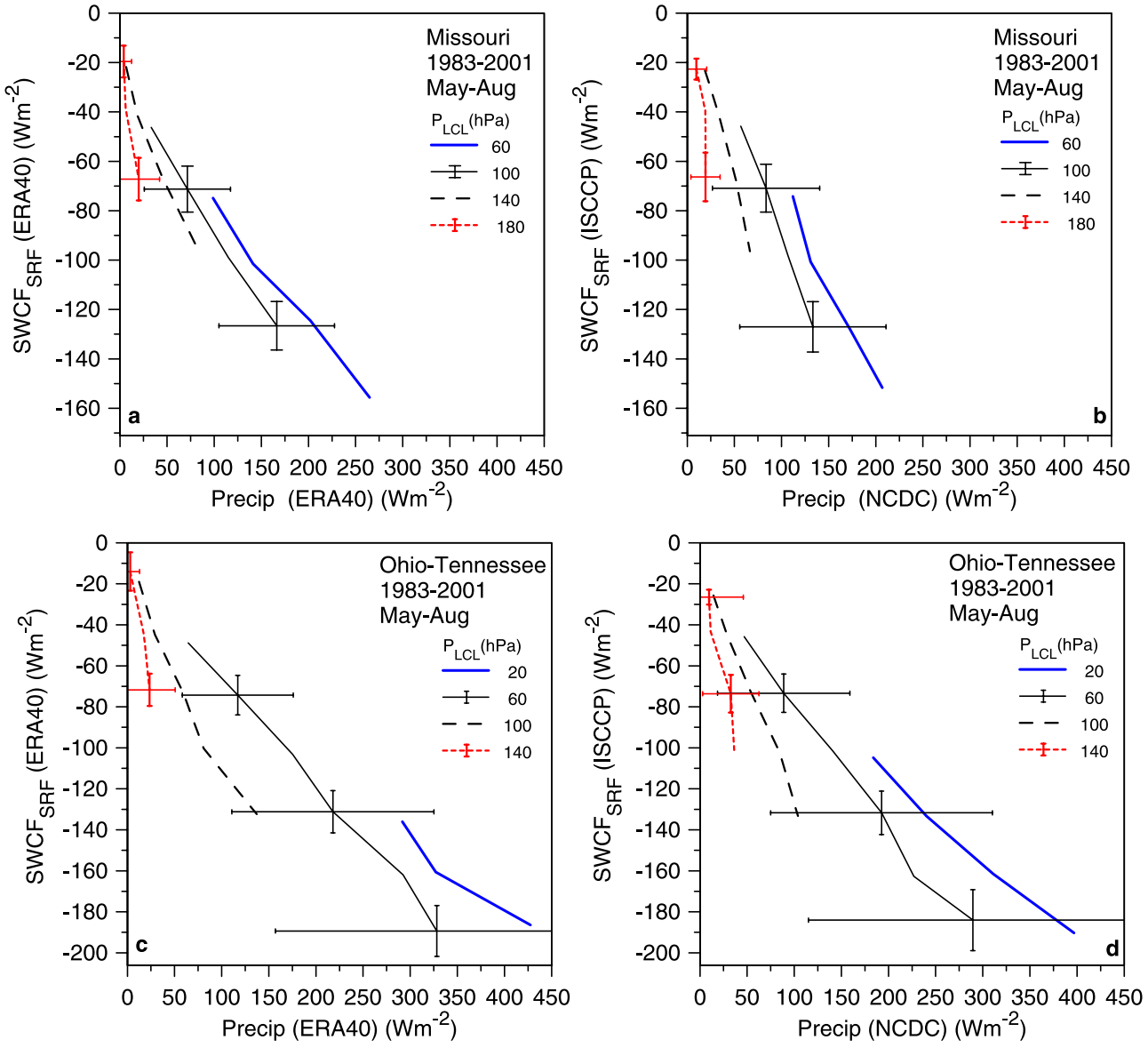

Figure 13. Relationship between precipitation diabatic forcing and surface SW radiative cloud forcing, stratified by α_{cloud} and P_{LCL} for ERA40 and observations.

in which the vegetation parameters are fixed at each grid point with no seasonal variation [*Van den Hurk et al.*, 2000].

6. Conclusions

[28] This paper compares ERA40 data with observations averaged over subbasins of the Mississippi, and integrated over the diurnal cycle, that is, on timescales of a day and space scales of order 800 km. The intent is to provide a framework for model diagnostics that can be evaluated against observations, and make some suggestions about further analysis strategies. Here, model short-wave fluxes have been compared with ISCCP data, and model precipitation with gridded surface observations. The effective cloud albedo at the surface, defined in terms of the surface SW cloud forcing, is proposed as a useful missing link that connects the cloud fields to both surface and large-scale processes. This definition removes the large seasonal variation of clear-sky fluxes associated with changing solar zenith angle. This surface cloud albedo is also closely related to the TOA SW cloud forcing, which is readily observed from space. The main simplification we have made is to reference these effective cloud albedos to the ERA40 clear-sky fluxes. On the daily timescale, basin mean cloud albedo for ERA40 and ISCCP are well correlated. However, except in summer, ERA40 has a systematic low bias in effective cloud albedo compared to ISCCP for all basins, and this bias is largest in winter, when it reaches –10%. This winter low cloud bias, which is seen on almost all days, suggests that the removal of cloud water and ice by large-scale precipitation processes is too efficient in ERA40. This cloud albedo bias on the basin scale, derived here from satellite data, has almost the same seasonal pattern as that derived by comparing ERA40 with direct measurements from three flux towers in central Saskatchewan [*Betts et al.*,

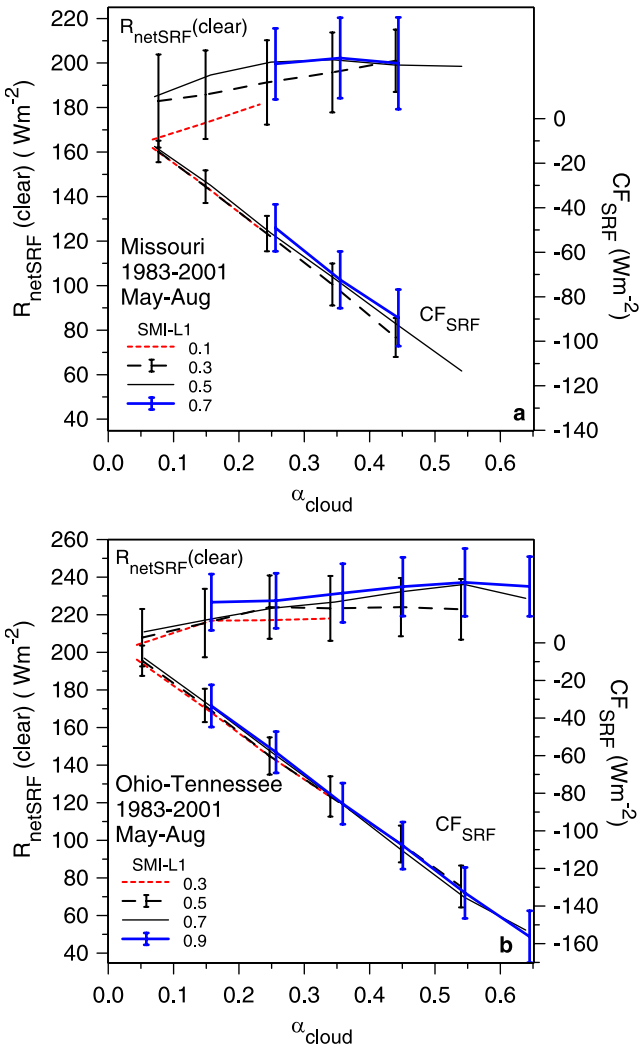

Figure 14. ERA40 surface clear-sky net radiation and cloud forcing as a function of α_{cloud} and soil moisture index for Missouri and Ohio-Tennessee.

2006a]. The seasonal bias in model cloud is not related to the seasonal bias in model precipitation, which varies between basins.

[29] The paper then looks at the coupling between processes in the warm season, starting with the interrelationship of soil moisture, lifting condensation level, RH and precipitation. The land-surface-atmosphere coupling in ERA40 is a two-way interaction, so that although the figures are suggestive of important couplings within the system on the daily timescale, they do not show a "direction of causality." On daily timescales, the LCL falls as soil moisture and precipitation increase. Soil moisture, especially in the upper soil layer responds directly to precipitation. Evaporation from the surface increases with increasing soil moisture (as well as when there is water in the skin reservoirs) and this increases RH and lowers the LCL. In addition the evaporation of falling precipitation lowers the LCL by bringing the subcloud layer closer to saturation, and this effect increases with increasing precipitation rate. In addition to these physical relationships, two aspects of the analysis constrain both soil moisture and the near-surface RH and LCL. The soil moisture analysis uses analysis increments of 2-m temperature and RH to control drifts of soil moisture, and during the daytime the surface RH observations are used directly in the atmospheric 3-D variational assimilation. Consequently, the height of the LCL (related closely to RH) is constrained by the surface humidity observations (in regions of data), so the ERA40 P_{LCL} was used to stratify the data from both reanalysis and observations.

[30] The increase of both cloud albedo and precipitation with moisture convergence and a lower LCL (cloud base) is similar in both reanalysis and observations. Consequently, both reanalysis and observations show a similar pattern when precipitation is plotted as a function of cloud albedo and cloud base. This stratification suggests that knowledge

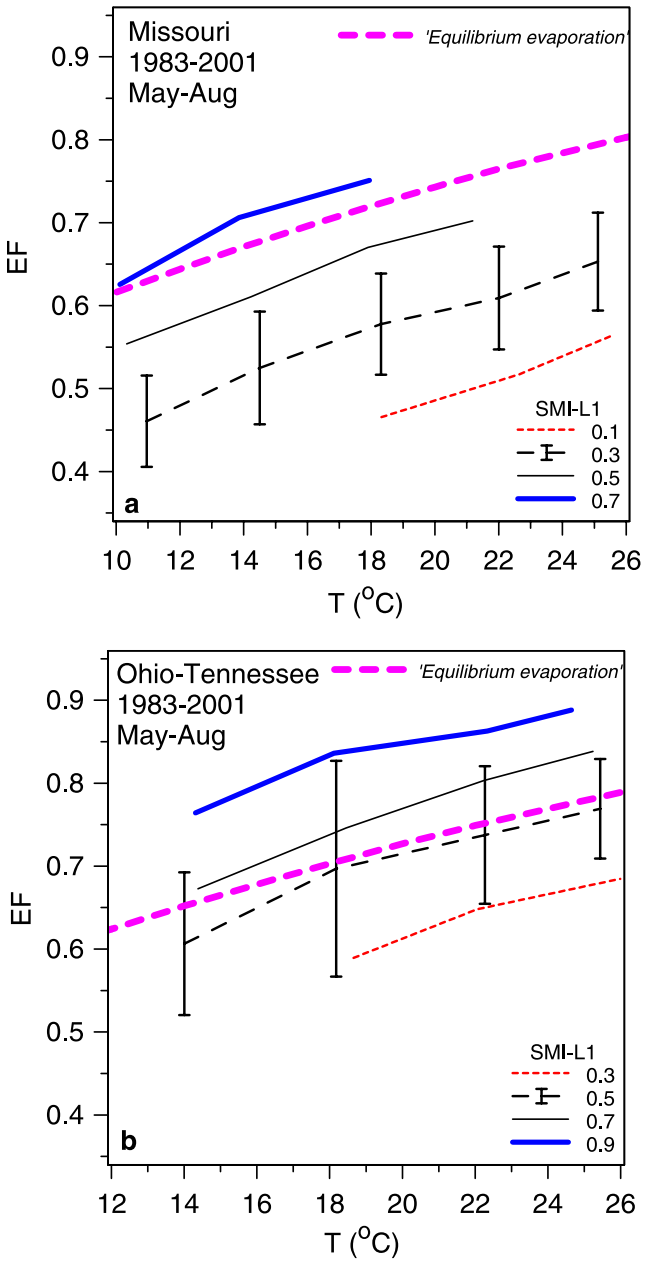

Figure 15. ERA40 EF as a function of temperature and soil moisture index for Missouri and Ohio-Tennessee.

of cloud base may improve estimates of precipitation from satellite data. The ratio of the surface SW cloud radiative forcing to the diabatic precipitation heating of the atmosphere, which is of importance to the model climate especially over land, also depends on cloud base. This ratio is lower in ERA40 than for the observations in summer, as well as in winter, when the model effective cloud albedo has a low bias.

[31] The surface energy budget was then split into the surface net radiation and the evaporative fraction. The surface net radiation depends on the clear-sky fluxes and the surface cloud radiative forcing, which depends on basin scales largely on the effective cloud albedo. Evaporative fraction in ERA40 is closely linked (with fixed vegetation parameters) to temperature and soil water. This would suggest that useful information on EF might be determined from temperature and microwave estimates of near-surface soil water.

[32] Cloud feedbacks are a major source of uncertainty in climate modeling, so a quantitative framework for their evaluation in terms of surface effective cloud albedo is likely to prove useful. This paper shows that ERA40 has identifiable biases in surface cloud albedo, which lead to a low bias in the ratio of the surface cloud SW radiative forcing to the diabatic precipitation heating of the atmosphere. It is also suggested that the mean cloud base height is useful for stratifying data on river basin scales, and that further exploration of the link between near-surface soil moisture and evaporative fraction (which is strong in ERA40) would be valuable.

[33] **Acknowledgments.** Alan Betts acknowledges support from NSF under grant ATM0529797, from NASA under NEWS grant NNG05GQ88A and from ECMWF for travel. He is grateful to Anton Beljaars and Pedro Viterbo for helpful discussions and to the entire ERA40 team for their assistance. Especial thanks to Bill Rossow and Y.-C. Chang for the basin-averaged ISCCP data and to Mike Bosilovich for the basin averaged precipitation data, derived from the U.S. Unified Precipitation data provided by the NOAA-CIRES Climate Diagnostics Center, available from http://www.cdc.noaa.gov/. Two reviews were helpful in improving the text.

References

Betts, A. K. (1997), The parameterization of deep convection, in *The Physics and Parameterization of Moist Atmospheric Convection*, edited by R. K. Smith, chap. 10, *NATO ASI Ser. C*, *505*, 255–279.

Betts, A. K. (2004), Understanding hydrometeorology using global models, *Bull. Am. Meteorol. Soc.*, *85*, 1673–1688.

Betts, A. K. (2006), Radiative scaling of the nocturnal boundary layer and the diurnal temperature range, *J. Geophys. Res.*, *111*, D07105, doi:10.1029/2005JD006560.

Betts, A. K., and C. Jakob (2002), Evaluation of the diurnal cycle of precipitation, surface thermodynamics, and surface fluxes in the ECMWF model using LBA data, *J. Geophys. Res.*, *107*(D20), 8045, doi:10.1029/2001JD000427.

Betts, A. K., and P. Viterbo (2005), Land-surface, boundary layer and cloud-field coupling over the south-western Amazon in ERA-40, *J. Geophys. Res.*, *110*, D14108, doi:10.1029/2004JD005702.

Betts, A. K., J. H. Ball, A. C. M. Beljaars, M. J. Miller, and P. Viterbo (1996), The land-surface-atmosphere interaction: A review based on observational and global modeling perspectives, *J. Geophys. Res.*, *101*, 7209–7225.

Betts, A. K., J. H. Ball, M. Bosilovich, P. Viterbo, Y. Zhang, and W. B. Rossow (2003a), Intercomparison of water and energy budgets for five Mississippi subbasins between ECMWF reanalysis (ERA-40) and NASA Data Assimilation Office fvGCM for 1990–1999, *J. Geophys. Res.*, *108*(D16), 8618, doi:10.1029/2002JD003127.

Betts, A. K., J. H. Ball, and P. Viterbo (2003b), Evaluation of the ERA-40 surface water budget and surface temperature for the Mackenzie River basin, *J. Hydrometeorol.*, *4*, 1194–1211.

Betts, A. K., J. H. Ball, P. Viterbo, A. Dai, and J. A. Marengo (2005), Hydrometeorology of the Amazon in ERA-40, *J. Hydrometeorol.*, *6*, 764–774.

Betts, A. K., J. Ball, A. Barr, T. A. Black, J. H. McCaughey, and P. Viterbo (2006a), Assessing land-surface-atmosphere coupling in the ERA-40 reanalysis with boreal forest data, *Agric. For. Meteorol.*, *140*, 355–382, doi:10.1016/j.agrformet.2006.08.009.

Betts, A. K., M. Zhao, P. A. Dirmeyer, and A. C. M. Beljaars (2006b), Comparison of ERA40 and NCEP/DOE near-surface datasets with other ISLSCP-II datasets, *J. Geophys. Res.*, *111*, D22S04, doi:10.1029/2006JD007174.

Cess, R. D., et al. (1990), Intercomparison and interpretation of cloud-climate feedback processes in nineteen atmospheric general circulation models, *J. Geophys. Res.*, *95*, 16,601–16,615.

Dirmeyer, P. A., R. D. Koster, and Z. Guo (2006), Do global models properly represent the feedback between land and atmosphere?, *J. Hydrometeorol.*, *7*, 1177–1198.

Douville, H., P. Viterbo, J.-F. Mahfouf, and A. C. M. Beljaars (2000), Evaluation of optimal interpolation and nudging techniques for soil moisture analysis using FIFE data, *Mon. Weather Rev.*, *128*, 1733–1756.

Eltahir, E. A. B., and E. J. Humphries (1998), The role of clouds in the surface energy balance over the Amazon forest, *Int. J. Climatol.*, *18*, 1575–1591.

Higgins, R. W., J. E. Janowiak, and Y.-P. Yao (1996), A gridded hourly precipitation data base for the United States (1963–1993), *NCEP/Climate Prediction Center Atlas*, *1*, Natl. Weather Serv., NOAA, U.S. Dep. of Commer., Washington, D. C.

Higgins, R. W., W. Shi, E. Yarosh, and R. Joyce (2000), Improved United States precipitation quality control system and analysis, *NCEP/Climate Prediction Center Atlas*, *7*, Natl. Weather Serv., NOAA, U.S. Dep. of Commer., Washington, D. C.

Kållberg, P., A. Simmons, S. Uppala, and M. Fuentes (2004), The ERA-40 archive, *ERA-40 Proj. Rep.*, *17*, 31 pp., Eur. Cent. for Med.-Range Weather Forecasts, Reading, U. K. (Available at http://www.ecmwf.int/publications/library/ecpublications/_pdf/era40/ERA40_PRS17.pdf)

McNaughton, K. G. (1976), Evaporation and advection I: Evaporation from extensive homogeneous surfaces, *Q. J. R. Meteorol. Soc.*, *102*, 181–191.

Morcrette, J.-J. (2002), Assessment of the ECMWF model cloudiness and surface radiation fields at the ARM SGP site, *Mon. Weather Rev.*, *130*, 257–277.

Pinker, R. T., et al. (2003), Surface radiation budgets in support of the GEWEX Continental-Scale International Project (GCIP) and the GEWEX Americas Prediction Project (GAPP), including the North American Land Data Assimilation System (NLDAS) project, *J. Geophys. Res.*, *108*(D22), 8844, doi:10.1029/2002JD003301.

Priestley, C. H. B., and R. J. Taylor (1972), On the assessment of surface heat flux and evaporation, *Mon. Weather Rev.*, *106*, 81–92.

Rossow, W. B., and Y.-C. Zhang (1995), Calculation of surface and top-of-atmosphere radiative fluxes from physical quantities based on ISCCP: 2. Validation and first results, *J. Geophys. Res.*, *100*, 1167–1197.

Smith, W. L., H. M. Woolf, C. M. Hayden, D. Q. Wark, and L. M. McMillin (1979), The TIROS-N operational vertical sounder, *Bull. Am. Meteorol. Soc.*, *60*, 117–118.

Uppala, S. M., et al. (2005), The ERA-40 reanalysis, *Q. J. R. Meteorol. Soc.*, *131*, 2961–3012.

Van den Hurk, B. J. J. M., P. Viterbo, A. C. M. Beljaars, and A. K. Betts (2000), Offline validation of the ERA-40 surface scheme, *ECMWF Tech Memo*, *295*, 43 pp., Eur. Cent. for Med.-Range Weather Forecasts, Reading, U. K. (Available at http://www.ecmwf.int/publications/library/ecpublications/_pdf/tm/001-300/tm295.pdf)

Zhang, Y.-C., W. B. Rossow, and A. A. Lacis (1995), Calculation of surface and top-of-atmosphere radiative fluxes from physical quantities based on ISCCP: 1. Method and sensitivity to input data uncertainties, *J. Geophys. Res.*, *100*, 1149–1165.

A. K. Betts, Atmospheric Research, Pittsford, VT 05763, USA. (akbetts@aol.com)